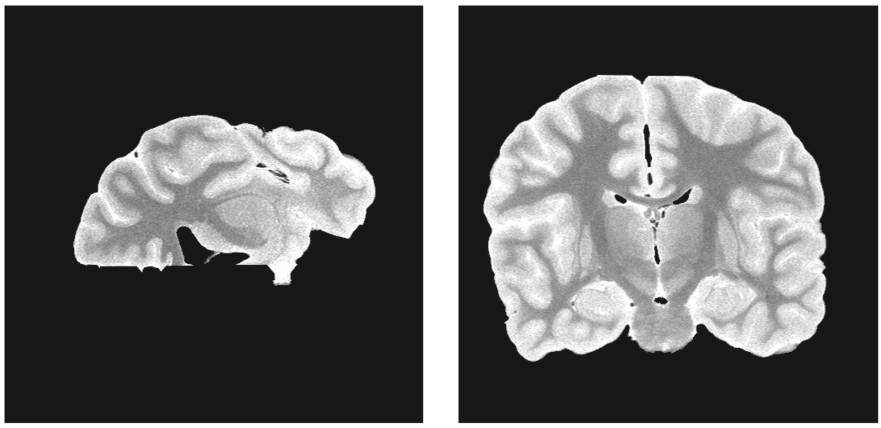

(a) (b)

Figure 1. Sample postmortem coronal slices: (a) slice 50 from half-brain of a control case; (b) slice 60 from whole brain of an autistic subject.

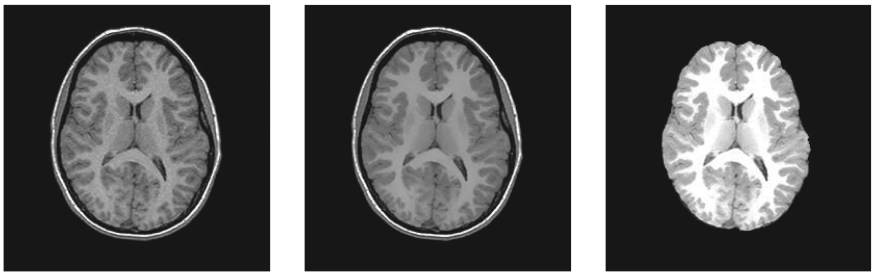

(a) (b) (c)

Figure 2. Smoothing and skull stripping results using the BET2/FSL software: (a) slice from original dataset: (b) smoothing results using the anisotropic filter: (c) skull stripping result. The slice is from the savant dataset corresponding to a normal female, 25 years of age.

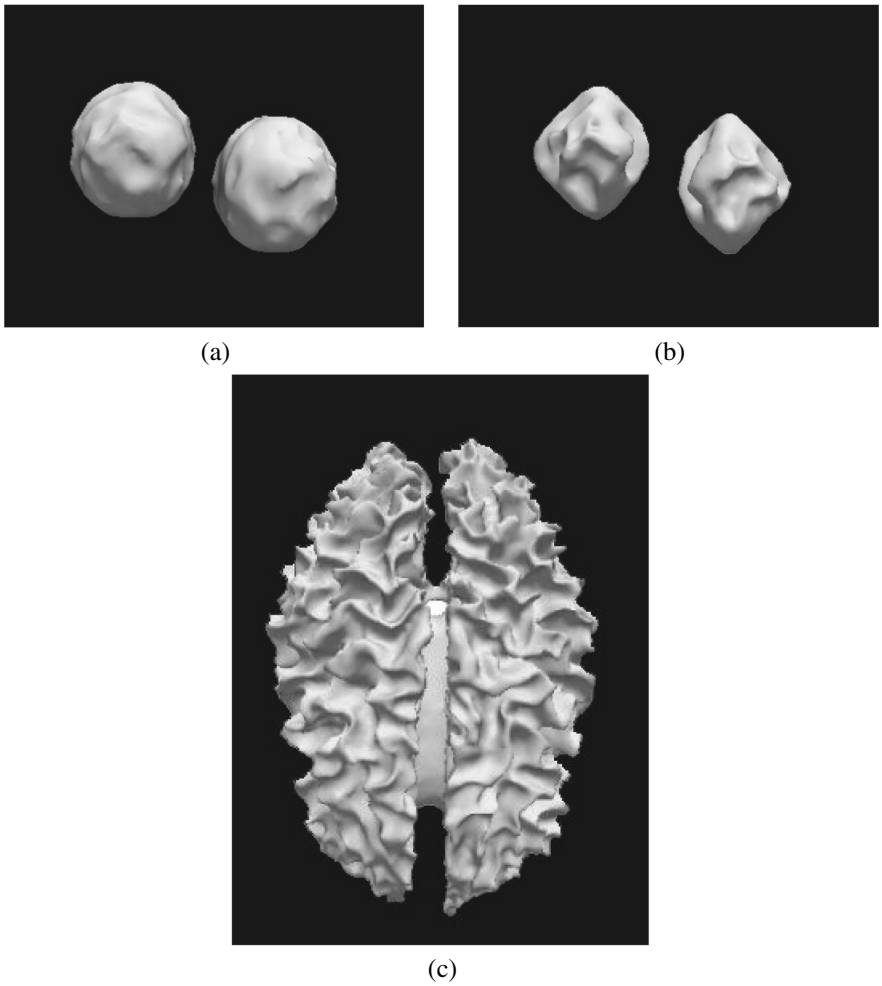

Figure 3. Several steps in a surface evolution to extract the white matter of the brain from an MRI scan: (a) initialization of the algorithm by two spheres inside the WM; (b) intermediate evolution step; (c) final result of the surface evolution representing the extracted WM volume.

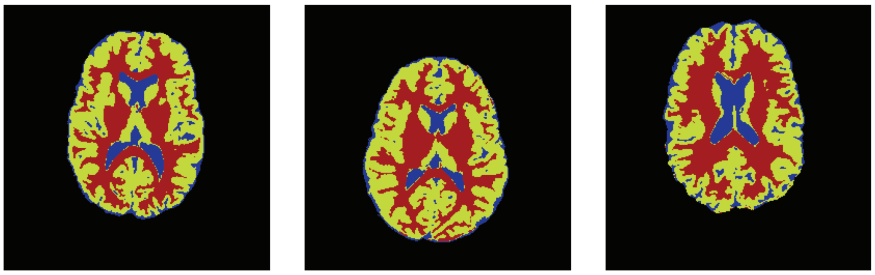

(a) (b) (c)

Figure 4. Some 2D displays of segmentation results (into WM, GM, CSF). Slice 69 from MRI scan of (a) an 68-year-old autistic female; (b) a 4-year-old autistic male; (c) a 34-year-old healthy male.

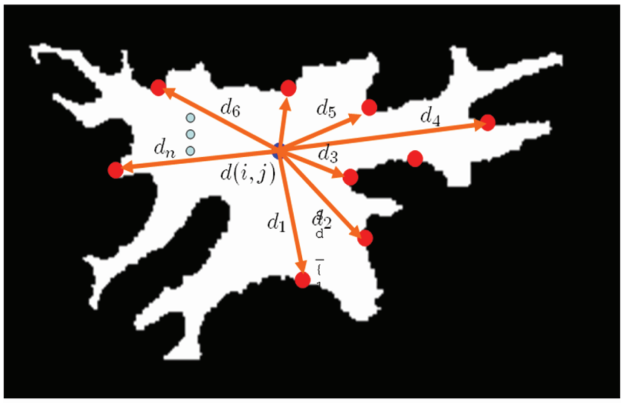

Figure 5. Distance map concept.

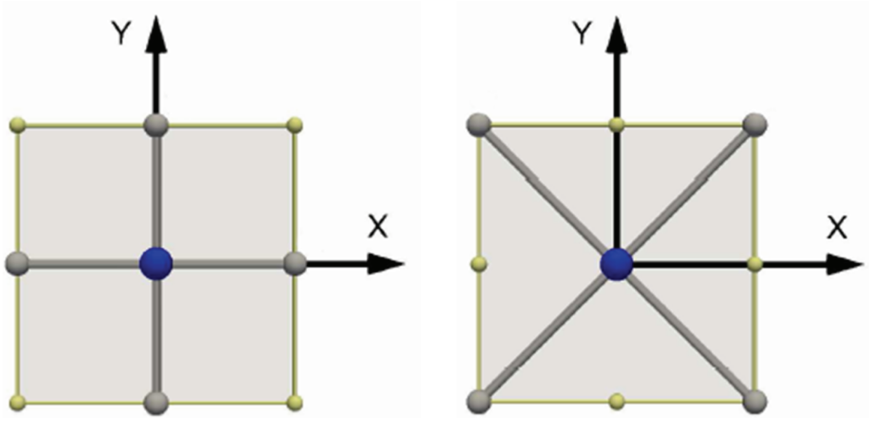

Figure 6. Proposed stencils for 2D Cartesian domain.

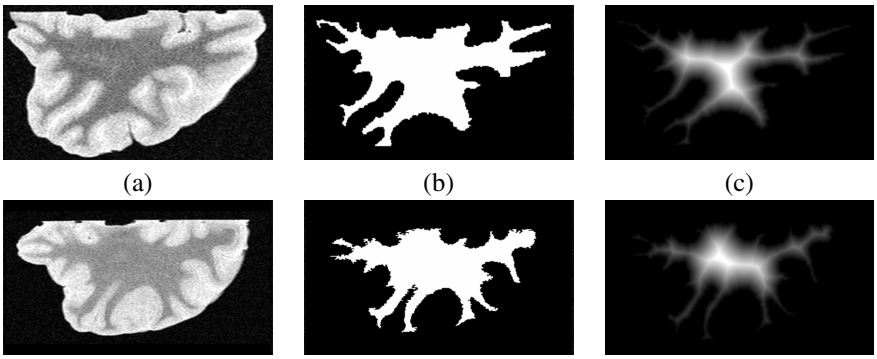

Figure 7. Left to right: 1st column = two typical MR slices from postmortem data; 2nd column = segmented white matter; 3rd column = distance maps inside the WM.

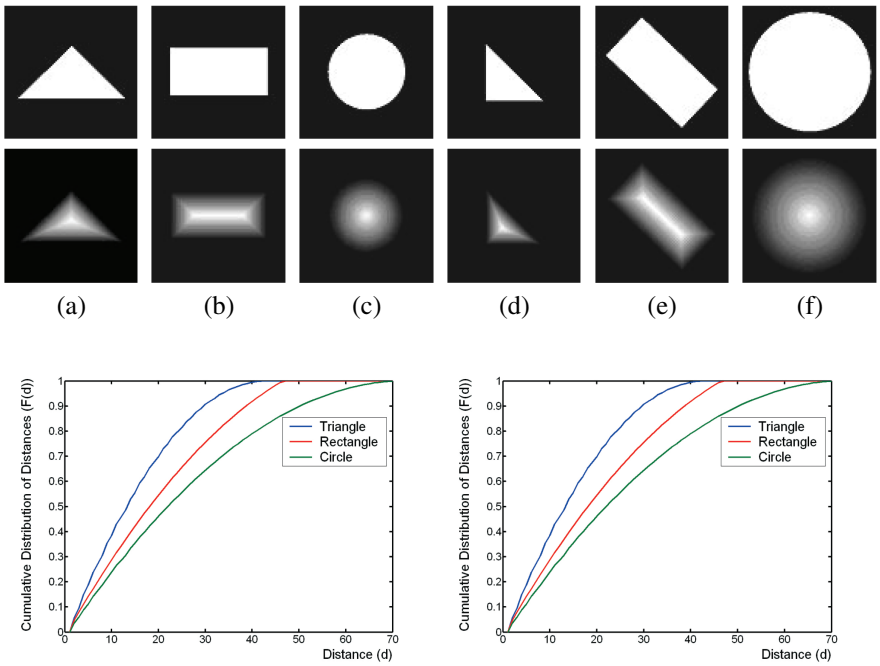

Figure 8. Illustration examples of using the cumulative distribution to discriminate between different shapes. From top to bottom: 1st row = six different objects; 2nd row = their corresponding distance maps computed by the proposed MSFM technique; 3rd row = CDFs of the left three shapes and those of the right three shapes.

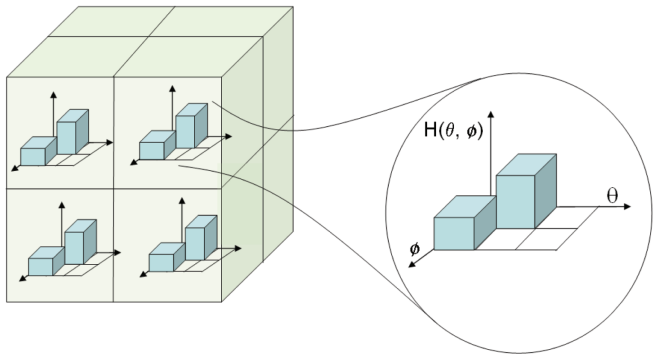

Figure 9. Structure of the 3D feature descriptor. Only eight samples of neighboring cells and six histogram bins are shown in the Figure for illustration purposes.

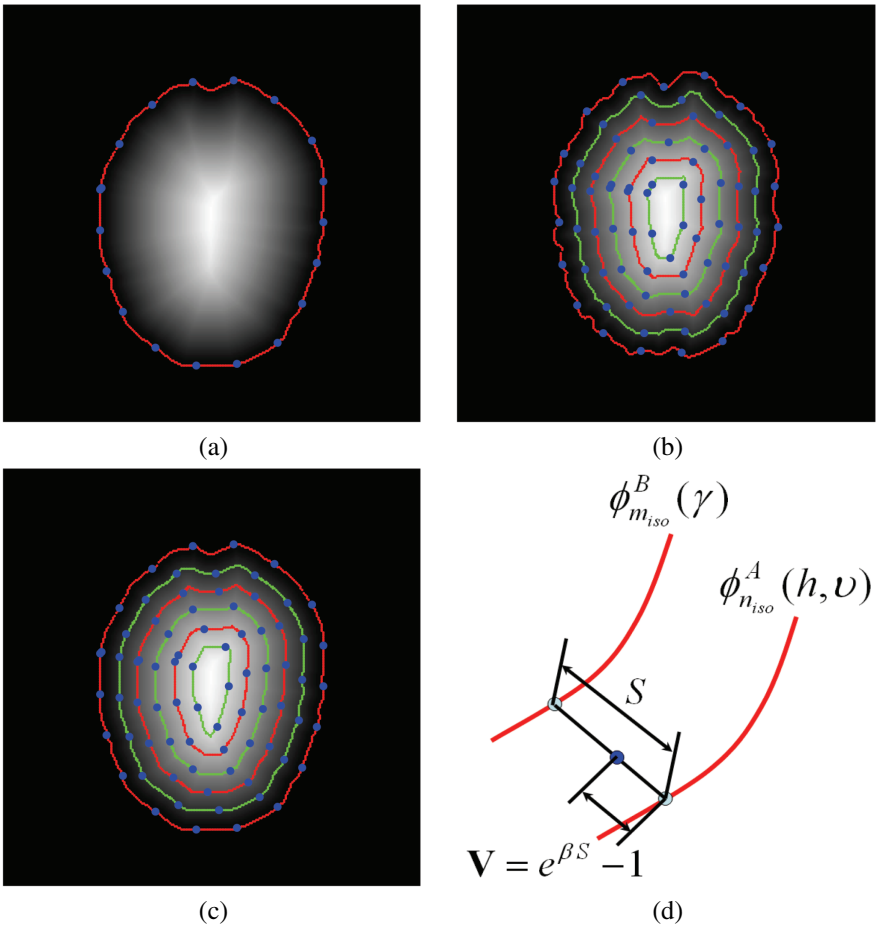

Figure 10. Cross-sectional views of generated distance map and iso-surfaces before (a) and after (b,c) deformation. The evolution scenario is depicted in (d).

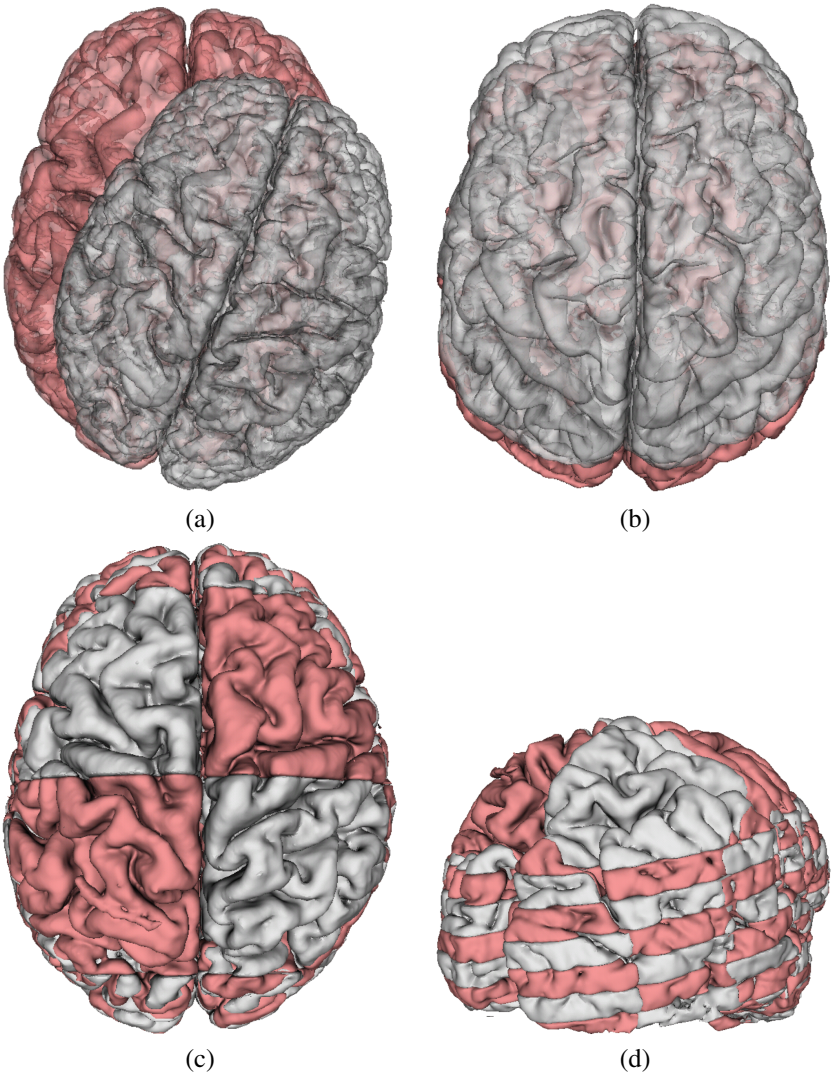

Figure 11. (a) The two volumes before alignment: (b) rigid alignment; (c,d) two different views after applying our nonrigid registration method [**?**].

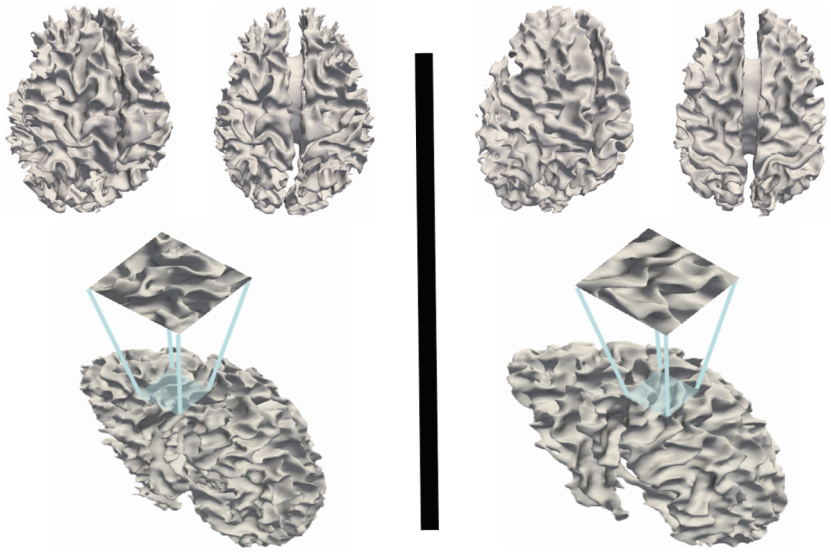

Figure 12. Different views of segmented white matter for autistic and normal subjects (savant data). Left, autistic; right, normal. Note that the gyrifications in autistic WM are thinner than those in normal WM. The zooms illustrate this difference in WM gyrification between the two groups.

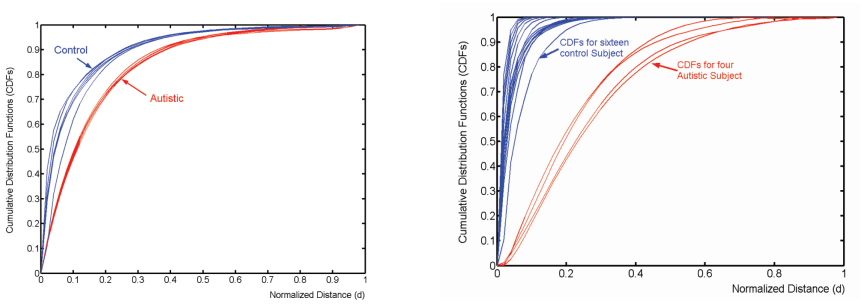

(a) (b)

Figure 13. (a) From postmortem data: distance map CDFs inside the WM of four autistic subjects and six controls. (b) From savant data: distance map CDFs inside the WM of four autistic subjects and sixteen controls.

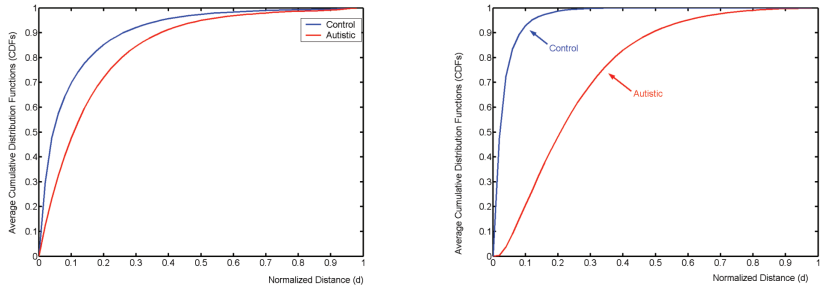

Figure 14. Average cumulative distribution functions inside the WM of four autistic subjects and six controls: (a) from postmortem data; (b) from savant data.

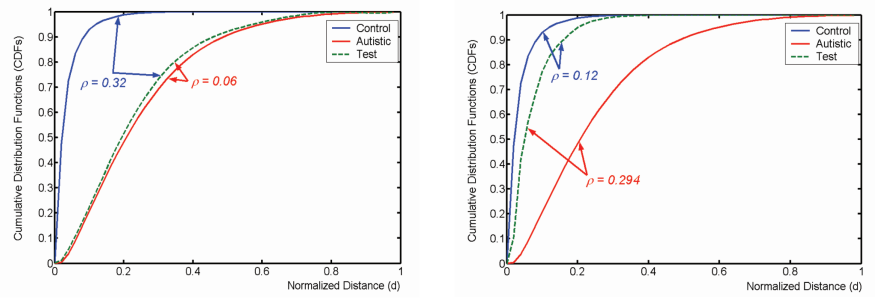

Figure 15. Illustration of using the proposed classification approach: (a) green CDF is classified as normal; (b) green CDF is classified as autistic. The parameter ρ denotes the Levy distance.

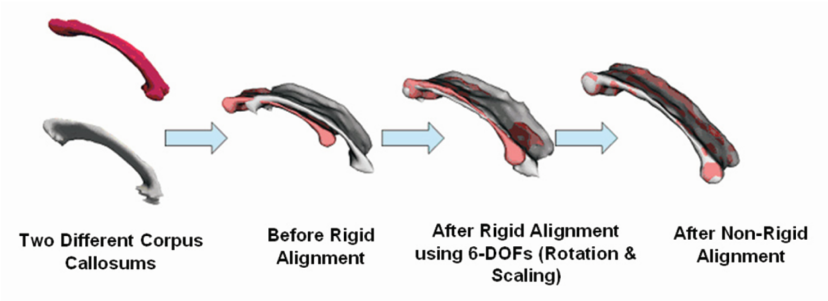

Figure 16. 3D registration of CC datasets using our nonrigid registration technique.

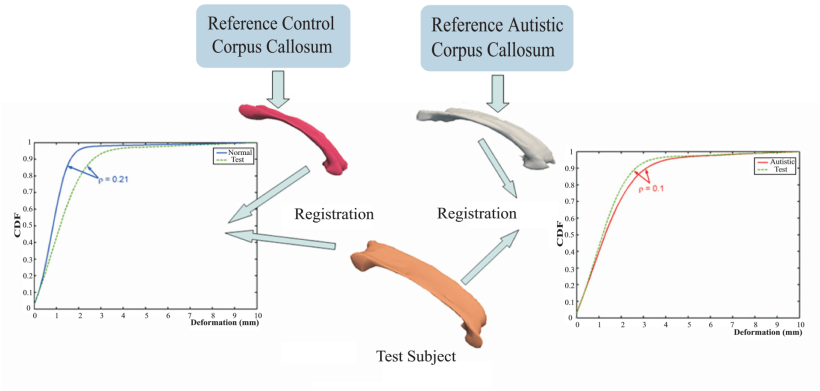

Figure 17. Illustration of CC registration-based classification approach. Parameter ρ denotes the Levy distance chosen to measure the difference between CDFs.

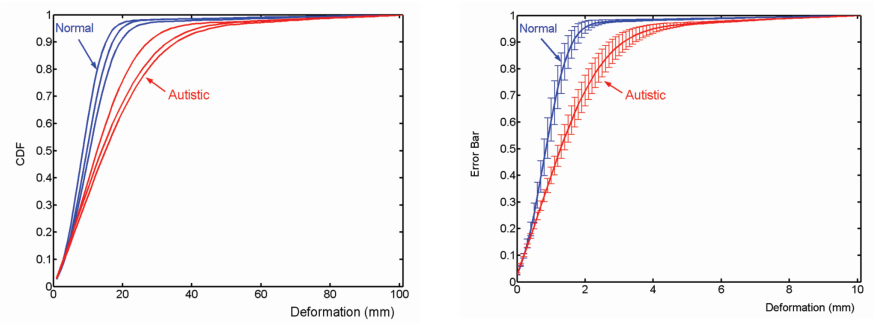

(a) (b)

Figure 18. (a) Cumulative distribution of displacement fields resulting from registration of 3 subjects to the reference within each group. (b) Error analysis showing the averages CDFs for each group.